ACS NANOSCIENCE Au
AN OPEN ACCESS JOURNAL OF THE AMERICAN CHEMICAL SOCIETY

pubs.acs.org/nanoau
Article

Tuning Chemical DNA Ligation within DNA Crystals and Protein−DNA Cocrystals

Abigail R. Orun, Caroline K. Slaughter, Ethan T. Shields, Ananya Vajapayajula, Sara Jones, Rojina Shrestha, and Christopher D. Snow*

Cite This: ACS Nanosci. Au 2024, 4, 338−348
Read Online
ACCESS | Metrics & More | Article Recommendations | Supporting Information

ABSTRACT: Biomolecular crystals can serve as materials for a plethora of applications including precise guest entrapment. However, as grown, biomolecular crystals are fragile in solutions other than their growth conditions. For crystals to achieve their full potential as hosts for other molecules, crystals can be made stronger with bioconjugation. Building on our previous work using carbodiimide 1-ethyl-3-(3-(dimethylamino)propyl)carbodiimide (EDC) for chemical ligation, here, we investigate DNA junction architecture through sticky base overhang lengths and the role of scaffold proteins in cross-linking within two classes of biomolecular crystals: cocrystals of DNA-binding proteins and pure DNA crystals. Both crystal classes contain DNA junctions where DNA strands stack up end-to-end. Ligation yields were studied as a function of sticky base overhang length and terminal phosphorylation status. The best ligation performance for both crystal classes was achieved with longer sticky overhangs and terminal 3′phosphates. Notably, EDC chemical ligation was achieved in crystals with pore sizes too small for intracrystal transport of ligase enzyme. Postassembly cross-linking produced dramatic stability improvements for both DNA crystals and cocrystals in water and blood serum. The results presented may help crystals containing DNA achieve broader application utility, including as structural biology scaffolds.

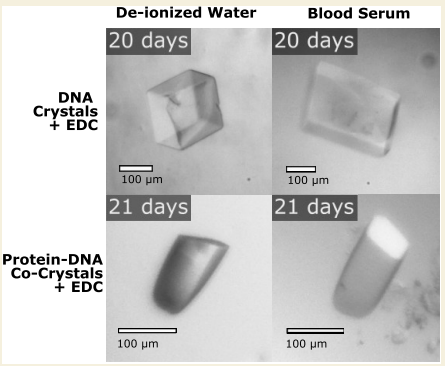

KEYWORDS: *cross-linking, ligation, DNA, cocrystal, X-ray diffraction*

INTRODUCTION

Crystals made from protein and DNA are versatile materials that precisely order molecules, self-assemble, and have tunable growth.[1−5] Porous crystals have been shown to act as molecular sieves[11−14] and to host molecules for structure determination,[6−9] enhance enzymatic activity,[10,11] and information storage via synthetic DNA sequences.[12] Engineered crystals with DNA building blocks, from pure DNA crystals[13,14] to hybrid protein−DNA crystals, have been designed to serve as scaffolds for DNA-binding molecules.[15−18] However, the broad utility of crystals held together by DNA is restricted by their ability to survive in varied solution conditions. As grown, crystals made from biological units are held together by weak noncovalent bonds and are likely to dissolve when introduced to anything other than their growth solution. Even more, crystals with DNA building units are particularly sensitive to changes in divalent cations. Crystal stability must be enhanced to fully realize the potential of crystals as biomaterials[19] and molecular scaffolds.[13,15,16]

Herein, we optimize a chemical DNA ligation strategy to provide stability for crystals containing DNA stacks (both pure DNA crystals and protein−DNA cocrystals). Enhanced stability makes crystals robust in water and blood serum for biomedical applications. The chemical ligation yields shown in DNA crystals set a record, exceeding previous biological ligation yields[20] and providing a method for crystalline DNA junction ligation less hindered by the crystal porosity or steric accessibility to the DNA−DNA junctions.

Bioconjugation, also called cross-linking in this context, is a technique to make crystals strong for application utility[21] by introducing covalent bonds between the neighboring units in the crystal. Cross-linking techniques for crystals containing DNA are established in the literature.[22−24] However, some established protocols involve highly reactive DNA cross-linking agents that introduce permanent links quickly but with unnatural bonds and severe safety challenges.[22]

An alternative DNA cross-linking strategy is ligation, a zero-length bond between neighboring DNA−DNA phosphate backbones (Figure 1B). In crystals where DNA lines up end-to-end, either with a blunt or sticky base overlap, ligation can heal the nick in the DNA. In other words, upon ligation, two neighboring duplexes become one contiguous piece of DNA. Under the right pH and solution conditions, chemical ligation

Received: April 22, 2024
Revised: June 10, 2024
Accepted: June 11, 2024
Published: June 25, 2024

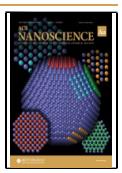

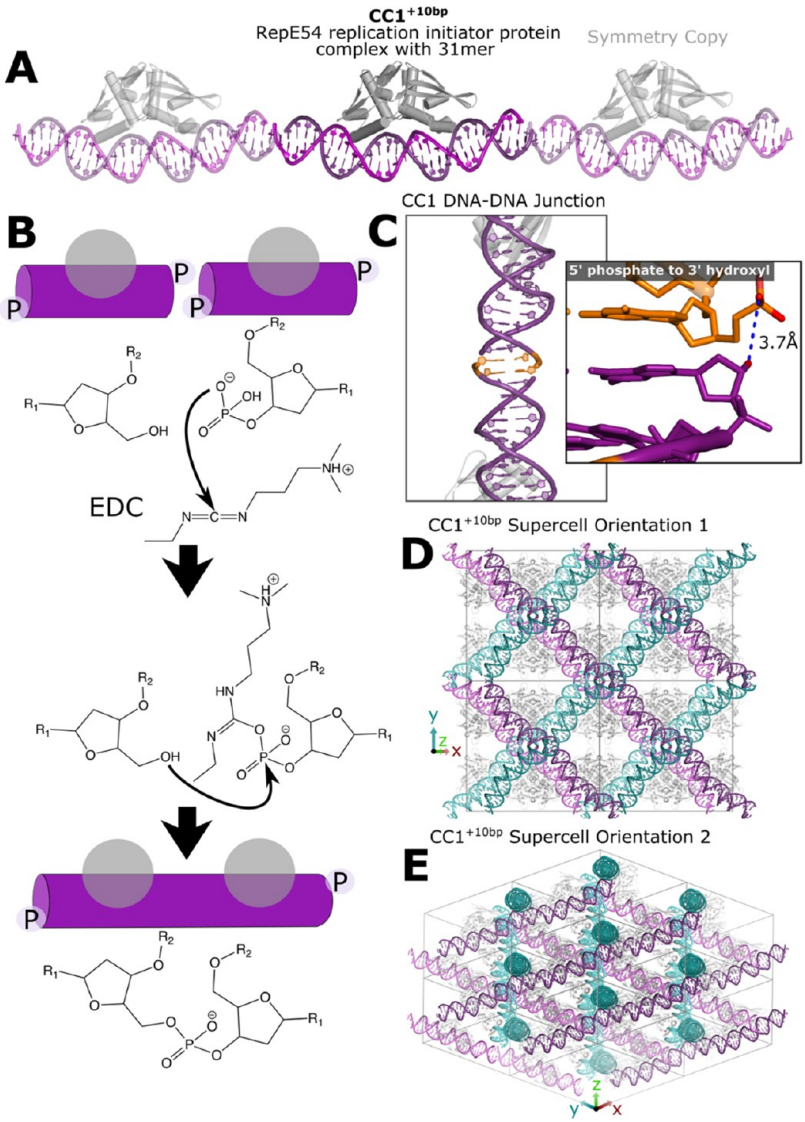

Figure 1. Protein−DNA cocrystal used to study the effects of sticky base overhang length on EDC ligation. (A) Replication initiator protein complexed to a 31mer cognate DNA sequence, named CC1^{+10bp}. (B) Putative mechanism for EDC ligation of DNA. R_1 is the nucleobase, and R_2 is the phosphate backbone. The schematic view of the DNA blocks in the crystal with terminal phosphates showing that upon ligation, the blocks become a single block of DNA. (C) DNA−DNA junction of CC1^{+10bp} with 2 sticky base overhangs and 5′ terminal phosphates (PDB code: 7rva). The distance between the 5′ phosphorus and the neighboring 3′ hydroxyl oxygen is measured in PyMOL as 3.7 Å. (D) Supercell orientation 1 shows four distinct versions of the DNA stack directions in the crystal, highlighted in four different colors (light cyan, dark cyan, light magenta, dark magenta). (E) Supercell orientation 2 shows another view of the four different DNA stack directions in the crystal.

can be achieved with the reactive carbodiimide cross-linker, 1-ethyl-3-(3-(dimethylamino)propyl)carbodiimide (EDC).[25] Notably, EDC ligation forms a zero-length cross-link, with the resulting structure being chemically identical to the enzymatic ligation achieved with T4 DNA ligase. EDC reacts with a phosphate to form an intermediate, and the leaving group departs upon attack by the hydroxyl on a neighboring strand, forming a healed phosphate bond and a contiguous strand of DNA (Figure 1B).

Recently, we reported EDC ligation in cocrystals containing stacking DNA blocks,[26] and qualitative EDC ligation was demonstrated in crystals composed of DNA tiles.[27] The current report addresses several remaining questions: Can we quantify EDC ligation in DNA tile crystals? What role do sticky base overhang length and phosphorylation status play in the ligation of cocrystal and DNA crystals?

Recently, we designed an expanded, interpenetrating cocrystal lattice to serve as a molecular scaffold.[18] These cocrystals of RepE54 protein and cognate DNA duplex are the template cocrystals used in this study (Figure 1A). The expanded cocrystals were crystallized with RepE54 protein and 31mer cognate DNA duplex, 10 additional base pairs than the original cocrystal, called CC1^{+10bp}. To study ligation yields with respect to variations in the junctions, we varied sticky overhang length (0, 1, 2, and 3 nt overhang) and terminal phosphorylation status (3′ or 5′ phosphate) at the DNA junction cartooned in Figure 1B. Despite the plethora of variations at the junctions, the cocrystals grew in the same *I*222 space group and contained the same contacts with symmetry copies (Table S1). Therefore, CC1^{+10bp} variants could be compared side-by-side for ligation yields.

It is not clear the extent to which protein−protein EDC conjugation is stabilizing CC1. There is the possibility of EDC-

https://doi.org/10.1021/acsnanoscienceau.4c00013
ACS Nanosci. Au 2024, 4, 338−348

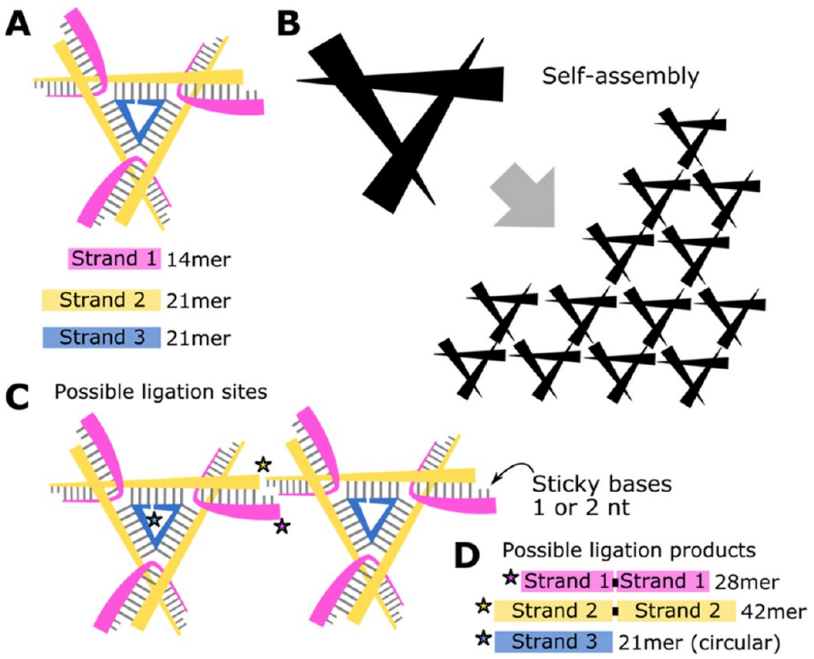

Figure 2. (A) Tensegrity triangle crystals are grown by mixing a stoichiometric ratio of three unique strands: Strand 1 (magenta), Strand 2 (yellow), and Strand 3 (blue). (B) Upon annealing, the DNA tiles self-assemble with sticky end cohesion at the DNA−DNA junctions. (C) At the sticky overhang region, selected possible ligation sites are labeled with stars. We varied the sticky base overhangs (1 or 2 nt) to study the effects on ligation yields. (D) Possible ligation products reflect polymerization of strand 1, polymerization of strand 2, or circularization of strand 3.

mediated protein−protein cross-linking across proximal carboxylic acid and primary amine groups.[21] Therefore, we sought to test the chemical ligation in the absence of protein using three-dimensional (3D) DNA crystals composed of three-armed tensegrity triangle tiles held together via sticky end cohesion.[2,13,14,28] As the DNA crystals only have DNA−DNA contacts, the only reaction with EDC should be DNA−DNA junction ligation. Each DNA tile has seven single strands: one central strand, three edge strands, and three crossover strands (Figure 2). Formerly, variations in the sticky end cohesion and overhang sequences were studied to improve the X-ray diffraction quality.[28] Here, we grew crystals with either 1 or 2 nt overhangs with sequences in Table S5 and Figure S3. At the DNA−DNA junctions, the strands stack such that upon ligation, crossover strands (S1) ligate to a flanking crossover strand (S1), resulting in ligation products S1−S1 (28mer), S1−S1−S1 (42mer), *etc.* The same ligation pattern occurs for the edge strands (S2), where a 21mer single edge strand becomes a 42mer double edge strand. The central strand (S3) simply ligates with itself to form a ring.

MATERIALS AND METHODS

Protein Cloning, Expression, and Purification

RepE54 initiator protein (CC1 protein) was expressed and purified by the Colorado State University Histone Source as described previously.[26] In short, the protein from PDB code 1rep was overexpressed with a N-terminal 6-Histag in *Escherichia coli* CodonPlus RIPL competent cells. Sonicated cell lysate was purified with Ni Excel Sepharose (Cytiva) and HiLoad Superdex 200 PG column (Cytiva). The resulting CC1 protein was concentrated to 15 mg/mL in storage buffer (100 mM sodium citrate pH 6.2, 100 mM KCl, 10 mM $MgCl_2$, and 10% glycerol) and stored at −80 °C after flash freezing with liquid nitrogen.

Oligonucleotides and Cocrystal Duplex Annealing

Strand 1, Strand 2, and Strand 3 oligomers were synthesized, and high-performance liquid chromatography (HPLC) was purified by Integrated DNA Technologies. DNA tensegrity triangle strands (Table S5) were resuspended in molecular biology grade water (VWR) and mixed with 3:3:1 stoichiometry to form a tile precursor solution at 60 μM. Annealing was achieved on the crystal plates in the DNA tile crystallization setup below. Cocrystal DNA duplexes are listed in Table S1. All 31-bp duplex sequences contained a conserved 19-bp iteron sequence for RepE54 protein−DNA binding but had varied sticky base overhang lengths and terminal phosphorylation status (no phosphate, 5′, or 3′ phosphate). The oligos were resuspended in 50 mM tris HCl and 100 mM KCl pH 7.0. Duplexes were annealed by combining cognate oligos 1:1, heating to 94 °C for 2 min, and then slowly cooling to room temperature over approximately 60 min. The final duplex concentrations were 4 mM. DNA stocks were quantified using a Qubit4 (Qubit 1 × dsDNA HS Assay Kit).

DNA−Protein Complex Cocrystallization

To grow cocrystals, protein and DNA were first combined (1:1.2 molar ratio), and the complex was incubated on ice for 30 min prior to the crystal plate setup. Cocrystals were then grown via sitting drop vapor diffusion in 24-well Intelli plates (Hampton Intelli-Plate 24-4 (Art Robbins 102-0004-00)) with 0.5 μL of protein−DNA complex and 0.5 μL of crystallization liquor. CC1 crystallization conditions were 300−500 mM $MgCl_2$, 25−35% PEG 400, and 100 mM tris HCl pH 8.0. Crystals grew to a span of 50−300 μm after 1 to 7 days.

DNA Tile Crystallization

The DNA crystals were grown using sitting drop vapor diffusion in Hampton 24-well Cryschem M plates. Crystals were grown by combining 14 μM DNA tile, 10−60 mM tris base pH 8.5, 5−30 mM acetic acid, 0.5−3 mM EDTA, and 125−750 mM magnesium acetate (exact crystallization conditions for each DNA tile variant are listed in Table S9). The precipitant was 1.75 M ammonium sulfate. Self-assembly was induced by incubating crystal plates at 60 °C for 10 min and then allowing crystals to cool to 25 °C over 1h in a Heratherm

https://doi.org/10.1021/acsnanoscienceau.4c00013
ACS Nanosci. Au 2024, 4, 338−348

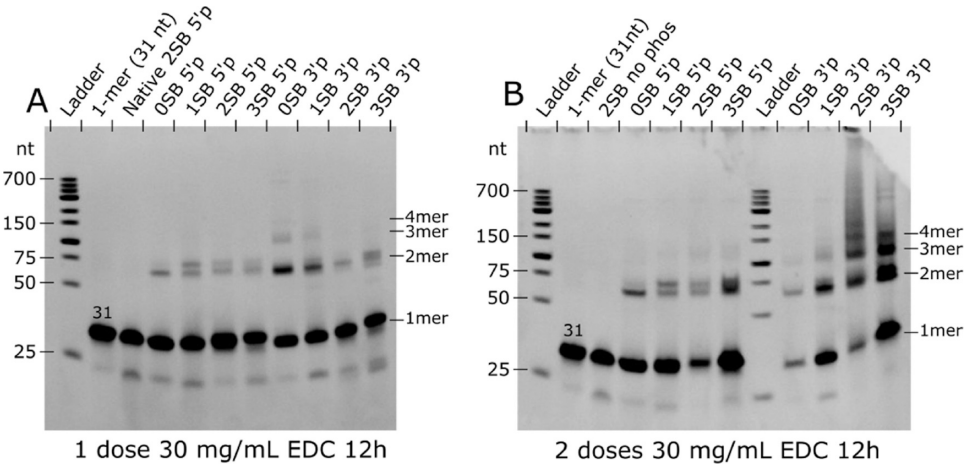

Figure 3. Ligation yield comparison for CC1 with varied sticky base overhang lengths and terminal phosphates. The TBE-urea gels of (A) CC1 after one EDC dose and (B) CC1 after two EDC doses. Additional ligation was achieved with longer sticky overhangs and 3′ phosphates after two doses. (A) 10% TBE-urea gel of CC1 illustrating a slightly improved ligation product distribution for 3′ vs. 5′ phosphates. (B) 10% TBE-urea gel of CC1 illustrating a dramatically improved ligation product distribution for 3′ vs. 5′ phosphates. Assigned band sizes are given in bp. Gel densitometry analysis and band attribution are provided in Figures S1 and S2.

Oven (Thermo Scientific). Crystals grew to a size of 25−200 μm after 1 to 3 days.

EDC Cross-Linking

Cocrystals and DNA crystals were washed prior to chemical EDC ligation to remove reactive buffer components (*i.e.*, primary amines, carboxylic acids), remove supernatant protein and/or DNA, and achieve optimal pH 6.0 for phosphate reactivity with EDC.[21] The CC1 wash condition consisted of 300−500 mM NaCl (substituting for $MgCl_2$), 25−35% PEG 400, and 100 mM MES pH 6.0 (substituting for tris HCl pH 8.0). The cocrystal wash completely avoids Mg(II), whereas in the DNA crystal wash, Mg(II) was still included until after the first EDC dose. The first DNA crystal wash conditions consisted of 10−60 mM MES pH 6.0 (substituting for tris base pH 8.5) and 125−750 mM $MgCl_2$ (substituting for magnesium acetate). In subsequent EDC doses, the magnesium was replaced fully with a wash solution consisting of 10−60 mM MES pH 6.0 and 125−750 mM NaCl.

Both cocrystals and DNA crystals were washed in 9-well glass plates (Hampton HR3-134) to remove additional protein and/or DNA monomers and unwanted buffer components. 1-Ethyl-3-(3-(dimethylamino)propyl)carbodiimide (EDC) (Advanced Chemtech CAS# 255952-53-8) was resuspended in the wash solution to 30 mg/mL and used immediately. The crystals were cross-linked in a 200 μL EDC solution volume for 12 h doses. The cross-linking reaction was quenched by moving crystals to 1× tris-borate-EDTA (TBE) buffer pH 8.3 containing 3.5 M urea.

DNA Gel Electrophoresis and Densitometry

Cross-linked cocrystals were dissolved in 1× TBE supplemented with 3.5 M urea and 20 μg of proteinase K and incubated at 50 °C for 12 h. The DNA crystals were dissolved in 3.5 M urea in 1× TBE and heated to 90 °C for 10 min. The crystals were analyzed with denaturing gels (10% Novex TBE-Urea Polyacrylamide Gel Electrophoresis) formulated with 7 M urea and run with 1× TBE running buffer. The cocrystal DNA ladder was the GeneRuler Low Range DNA Ladder (Thermo Scientific). Gels were incubated with 3× GelRed Nucleic Acid Gel Stain and imaged with a UVP Bioimaging System on the ethidium bromide setting. For gel densitometry, we used the technique established in our previous ligation study (Python scripts for fitting densitometry peaks with Gaussians).[26,29] The raw band intensity fits are provided in Tables S2, S6, and S8, and the densitometry fits using Gaussians are provided in Figures S1−S2 and S7−S8.

Stability Assays

Crystals were cross-linked with 2 doses of 30 mg/mL EDC, and the EDC reaction was quenched in 50 mM tris base pH 8.0 for 30 min. The crystals were equilibrated in cross-linking wash solution for 30 min prior to looping to stringent conditions. The stability test buffers used were as follows: molecular biology grade water (CORNING), very low pH 2.0 0.01 M HCl buffer (to mimic stomach acid), a moderately low pH 4.5 citrate buffer (46 mM sodium citrate, 54.1 mM citric acid to mimic lysosomal fluid pH), and blood serum (HyClone, bovine calf blood serum). Microscope images for each trial are provided in Figures S10−S15.

X-ray Diffraction Data Collection and Refinement

Single-crystal X-ray diffraction (XRD) data were collected for $CC1^{+10bp}$ cocrystals containing blunt ends, 1-nt, 2-nt, and 3-nt sticky base overhangs with 5′ or 3′ phosphates. As a control, XRD was obtained for a control cocrystal with 2-nt sticky base overhangs and no terminal phosphates. Crystals were cross-linked with 2 doses of 30 mg/mL EDC for 12 h and flash frozen directly from EDC cross-link (no quench) for XRD. Data sets were collected at the Advance Light Source Beamline 4.2.2. on a CMOS detector from 0 to 180° with omega delta 0.2 and 0.3 s exposure time. Data processing relied on XDS,[30] and refinement resolutions (Table S4) were defined by a cutoff of I/Sigma(I) > 1.5. Each structure was solved by molecular replacement using $CC1^{+10bp}$ with 2 sticky base overhangs and 5′ terminal phosphates (PDB code 7u6k)[18] and refined in PHENIX[31] and COOT[32] using the same Rfree flags as the previous $CC1^{+10bp}$ structures. Protein data bank entries for each cocrystal are found in Table S4, and X-ray diffraction and refinement statistics for all structures are provided in Tables S10−S15. The $CC1^{+10bp}$ 2SB 3′phosphate structure was refined with a bond length restraint (1.59 Å, the ideal DNA backbone phosphate-oxygen bond length)[33] at the terminal 3′P and flanking 5′OH.

RESULTS AND DISCUSSION

Chemical Ligation in Cocrystals

In our first study of EDC ligation templated by cocrystals,[26] two example cocrystals in which the DNA stacks up end-to-end were used as preliminary examples for *in crystallo* EDC ligation. One of these ligation targets, cocrystal 1 (CC1), was the cocrystal of replication initiator protein RepE54 and cognate DNA sequence. The original instance of CC1 (RepE54 and 21mer with 3′ dangling T's) contained DNA

https://doi.org/10.1021/acsnanoscienceau.4c00013
ACS Nanosci. Au 2024, 4, 338−348

duplexes stacking end-to-end. This original crystal structure was improved from 2.6 Å (PDB code: 1rep)[34] to 1.89 Å (PDB code: 7rva).[26] For the purposes of studying ligation in cocrystals, the original dangling T's were truncated to make a blunt-ended 21mer (PDB codes: 7sgc and 7sdp). The blunt-ended CC1 was a canvas to study chemical EDC ligation in cocrystals and the role of terminal phosphates. The blunt-ended junction was decorated with 5′ or 3′ terminal phosphates and underwent EDC cross-linking postcrystallization. In the case of CC1, the 3′ terminal phosphates ligated more readily than 5′ phosphates. Our next question became what is the role of sticky base overhangs in EDC ligation?

First, a gentle buffer exchange from the crystallization conditions to a cross-linking wash was necessary to remove compounds that interfere with EDC ligation and supernatant protein−DNA monomers. Three components of the $CC1^{+10bp}$ crystallization conditions (300−500 mM $MgCl_2$, 25−35% PEG 400, and 100 mM tris HCl pH 8.0) were modified. First, divalent cations were previously found to interfere with cocrystal ligation.[26] Therefore, Mg(II) was replaced 1:1 stoichiometrically with Na(I). Second, to adjust the pH from 8.0 to 6.0 to increase the phosphate reactivity with EDC,[21] the main crystallization buffer, tris HCl, was replaced with MES hydrate. After a buffer exchange, the crystals maintained their visible macroscopic structure and were transferred to cross-link wash containing EDC for ligation.

Parallel cross-linking trials were performed for crystals with varied sticky base overhang lengths and terminal phosphorylation status. Crystals were cross-linked with the optimal EDC ligation conditions found previously[26] (30 EDC mg/mL for 12 h), and the results were compared after one and two doses of EDC (Figure 3). We hypothesized that longer sticky base overhangs would improve EDC ligation yields because the sticky end cohesion would correctly orient the phosphate and flanking hydroxyl for the EDC reaction. The ligation yields (Figure 3 and Table 2) were quantified with TBE-urea gel electrophoresis and gel densitometry (our custom Python scripts published on Zenodo[29]) and ligation product calculations (Table 1). Briefly, we used Gaussian peak fitting

Table 1. Equations Used for Ligation Product Calculations[a]

Equation 1	$P_{SSB} = 1/\sum_i i \cdot x_i$	(1)
Equation 2	$P_{LIG} = 1 - P_{SSB}$	(2)
Equation 3	$P_{DSB} = (P_{SSB})^2$	(3)
Equation 4	$P_{DLIG} = (P_{LIG})^2$	(4)

[a]See the prior cocrystal ligation paper for derivations.[26]

to obtain estimated mole fractions (correcting for DNA length) for each DNA species (unfused, 2-mer, 3-mer, etc.) from the gel densitometry data. From these mole fractions, we can compute the total number of single-stranded breaks (SSB) per eq 1 (Table 1). A derivation can be found in the Supporting Information of the prior report.[26] The probability of ligated junctions (P_{LIG}) follows logically (eq 2). The probabilities that nonligation sites occur at the same junction leading to a double strand break (P_{DSB}) or double ligation sites at the same junction (P_{DLIG}) are given by eqs 3 or 4, assuming independence.

Figure 3A shows the first dose of EDC ligation with varied sticky base overhangs (0, 1, 2, and 3 nt.) and phosphorylation (5′P vs. 3′P). Independent of sticky base overhang length, the 3′phosphates had higher ligation yields than 5′ phosphates. Better yields with 3′ terminal phosphates over 5′ terminal phosphates in the blunt-ended $CC1^{+10bp}$ (zero sticky bases) concurred with our findings in the native, blunt-ended CC1 crystals.[26] After EDC dose 1, the 0SB and 1SB with 3′ terminal phosphates had slightly better yields than the 2SB and 3SB. After two EDC doses, the beneficial effects of sticky overhangs became more prominent, especially for the 3′phosphates. After the second dose of EDC, the 2SB overhang crystal yielded the highest ligation product for the $CC1^{+10bp}$ crystal variants, with ∼61% ligation (Table 2).

To further assess how the EDC ligation affects the nanoscale stability of the cocrystals, we obtained X-ray diffraction structures of cocrystals before and after EDC ligation (Table S4). On average, cocrystals after 2 doses of ligation lost ∼0.5 Å resolution. Also, the 3SB crystals were not diffracting; these crystals were small for XRD (∼30 μm span), and the native crystals were hit-or-miss in diffraction quality. Although no protein−protein cross-links stood out in the electron density, further studies could assess the EDC cross-linking in the protein of the cocrystals.

At the DNA−DNA junction, the $CC1^{+10bp}$ 2SB 3′ terminal phosphate structure (PDB code 8tj1) showed 61% ligation yield by densitometry. Therefore, the junction was refined with bond length restraints to represent a ligated junction. We were able to see electron density consistent with ligation in our previous paper[26] despite a modest resolution of 3.28 Å after 2 EDC cross-link doses. Here, we attempted to repeat this feat and obtained X-ray data sets on crystals subjected to the most stringent ligation conditions (i.e., CC1 2SB 3′phos). While the new crystals diffracted to a modest yet reasonable resolution after ligation (3.15 Å), we did not see clear contiguous electron density at the junction. In particular, the DNA−DNA junction for Chain A was not cleanly enveloped by electron density despite using a complete model with terminal phosphates (Figure S16). While we lack an obvious cause for unclear electron density in this instance, there are multiple possible causes for disorder at this location. First, the DNA/DNA junction is the most isolated/solvent-exposed part of the structure and has the highest B-factors. Second, the chemical ligation procedure does not result in 100% ligation across the junction. Rather, per Table 2 densitometry results, we expect only 61% of the junctions in CC1 2SB 3′phos crystals to have undergone ligation. Thus, the patchy electron density at this location may reflect the existence of a heterogeneous population of multiple chemical species (i.e., ligated and unligated) and multiple conformations thereof.

Chemical Ligation in DNA Crystals

To assess the role of sticky base overhang length and terminal phosphorylation status in DNA crystals, DNA crystals were grown with varied sticky base overhang lengths (1 and 2 SB) and varied terminal phosphates (5′ or 3′) (see Figure S3 and Table S5 for DNA tile sequences). To study the ligation yields at a single junction, the terminal phosphates were solely added to the crossover strands (S1(5′P or 3′P)-S2-S3). Then, we explored the ligation yields when all three strands were phosphorylated (S1(5′P or 3′P)-S2(5′P or 3′P)-S3(5′P or 3′P)).

As with the cocrystals, the first step for DNA crystal ligation was a gentle buffer exchange. The DNA tile crystallization conditions (10−60 mM tris base pH 8.5, 5−30 mM acetic

https://doi.org/10.1021/acsnanoscienceau.4c00013
ACS Nanosci. Au 2024, 4, 338−348

Table 2. Distribution of DNA Block Sizes as a Function of Crystal Sticky Base Overhang Length and 3′ vs. 5′ Terminal Phosphates[a]

Cocrystals EDC Dose One (Figure 3A)								
parent cocrystal	0SB 5′P	1SB 5′P	2SB 5′P	3SB 5′p	0SB 3′P	1SB 3′P	2SB 3′P	3SB 3′p
DNA block size	[%]	[%]	[%]	[%]	[%]	[%]	[%]	[%]
1	92.9	91.8	94.6	93.4	77.4	85.1	94.1	93.4
2	7.1	8.2	5.4	6.6	19.8	13.6	5.7	6.5
3					2.1	0.6	0.2	0.1
4					0.3	0.1		
5					7×10^{-9}		0.1	
6					0.1	0.2		
7					0.2	0.2		
8					0.2	0.1		
Parent Cocrystal	0SB 5′P	1SB 5′P	2SB 5′P	3SB 5′P	0SB 3′P	1SB 3′P	2SB 3′P	3SB 3′P
P_{SSB}[b]	0.93 ± 0.01	0.92 ± 0.01	0.95 ± 0.01	0.94 ± 0.01	0.77 ± 0.02	0.82 ± 0.03	0.94 ± 0.02	0.93 ± 0.02
$P_{LIG} = 1 - P_{SSB}$	0.07 ± 0.01	0.08 ± 0.01	0.05 ± 0.01	0.06 ± 0.01	0.23 ± 0.02	0.18 ± 0.03	0.06 ± 0.02	0.07 ± 0.02
$P_{DSB} = (P_{SSB})^2$	0.87 ± 0.02	0.85 ± 0.02	0.90 ± 0.02	0.88 ± 0.02	0.59 ± 0.04	0.68 ± 0.04	0.88 ± 0.03	0.87 ± 0.03
$P_{DLIG} = (P_{LIG})^2$	$4 \pm 2 \times 10^{-3}$	$6 \pm 2 \times 10^{-3}$	$3 \pm 1 \times 10^{-3}$	$4 \pm 2 \times 10^{-3}$	0.05 ± 0.01	0.03 ± 0.01	$4 \pm 2 \times 10^{-3}$	$5 \pm 2 \times 10^{-3}$
Cocrystals EDC Dose Two (Figure 3B)								
parent cocrystal	0SB 5′P	1SB 5′P	2SB 5′P	3SB 5′p	0SB 3′P	1SB 3′P	2SB 3′P	3SB 3′p
DNA block size	[%]	[%]	[%]	[%]	[%]	[%]	[%]	[%]
1	90.9	92.6	83.1	92.2	78.0	82.3	42.4	61.3
2	7.1	6.5	14.4	7.0	18.1	13.9	23.6	23.0
3	0.8	0.3	1.1	0.3	2.6	2.8	16.2	8.0
4	0.6	0.2	1×10^{-8}	0.2	0.5	0.4	5.9	3.8
5	0.1	0.2	0.2	0.03	2×10^{-8}	0.1	4.3	1.44
6	0.2	0.2	0.5	0.1	0.2	0.1	2.6	0.8639
7	0.1	0.1	0.3	0.03	0.1	0.2	1.5	0.6
8 and above	0.1		0.3	0.12	0.44	0.19	3.5	1.1
Parent Cocrystal	0SB 5′P	1SB 5′P	2SB 5′P	3SB 5′P	0SB 3′P	1SB 3′P	2SB 3′P	3SB 3′P
P_{SSB}[b]	0.86 ± 0.03	0.89 ± 0.03	0.79 ± 0.03	0.84 ± 0.04	0.73 ± 0.03	0.77 ± 0.03	0.39 ± 0.01	0.57 ± 0.02
$P_{LIG} = 1 - P_{SSB}$	0.14 ± 0.03	0.11 ± 0.03	0.21 ± 0.03	0.16 ± 0.04	0.27 ± 0.03	0.23 ± 0.03	0.61 ± 0.01	0.43 ± 0.02
$P_{DSB} = (P_{SSB})^2$	0.74 ± 0.05	0.78 ± 0.05	0.62 ± 0.05	0.70 ± 0.06	0.53 ± 0.04	0.59 ± 0.04	0.15 ± 0.01	0.33 ± 0.02
$P_{DLIG} = (P_{LIG})^2$	0.02 ± 0.01	0.01 ± 0.01	0.04 ± 0.01	0.03 ± 0.01	0.08 ± 0.02	0.05 ± 0.01	0.37 ± 0.02	0.18 ± 0.02

[a]Data shown correspond with the gel lanes in Figure 3. The cross-linking protocol was either 1 dose or 2 doses of 30 mg/mL EDC for 12 h. The values in this table are weighted, dividing by DNA length to account for the increased dye intensity with the DNA length. Unweighted values are found in Table S2. The full table including estimated mole fractions for higher-order products is found in Table S3. $P_{\text{Single Strand Break (SSB)}}$, $P_{\text{Ligation (LIG)}}$, $P_{\text{Double Strand Break (DSB)}}$, and $P_{\text{Double Ligation (DLIG)}}$ were calculated for each cross-linked crystal sample. Probabilities of double strand breaks or double strand ligations assume that ligation events are independent. P_{SSB} uncertainties are the standard deviation in the calculated P_{SSB} after 500 trials in which simulated noise (standard deviation 0.03) was introduced into relative band intensities. [b]Calculated from experimental mole fractions per eq 1 (Table 1). PLIG is derived from PSSB as shown.

acid, 0.5−3 mM EDTA, and 125−750 mM magnesium acetate) were assessed for EDC ligation favorability. The same concepts were applied: remove reactive species such as amines and carboxylic acids that hamper EDC ligation and make the solution conditions conductive to EDC ligation. In the resulting wash solution, we replaced tris base pH 8.5 with stoichiometric equivalent MES hydrate pH 6.0 for optimal phosphate reactivity. We also removed EDTA and acetic acid. Finally, we replaced magnesium acetate with a 1:1 stoichiometric equivalent magnesium chloride. In the end, the DNA crystal ligation wash buffer only contained 10−60 mM MES pH 6.0 and 125−750 mM magnesium chloride with concentrations matching the original growth condition concentrations of tris base and magnesium acetate, respectively. The DNA crystals maintained their visible macroscopic structure and were subsequently cross-linked in a wash solution supplemented with 30 mg/mL EDC.

Before comparing ligation yields, we determined if magnesium hindered DNA crystal ligation yields. Buffer exchange to fully remove Mg(II) could not be done without destroying the as-grown DNA crystals. Therefore, the first dose of EDC ligation was performed with magnesium present, and a subsequent dose was completed after a stoichiometric 1:1 replacement of Mg(II) with Na(I). When we replaced Mg(II) with Na(I), the ligation yields increased significantly for DNA crystals containing 5′ phosphates (Figures S4 and S5). However, after four doses of EDC, there was no quantitative difference in ligation yields (Table 3) for repeated ligation in magnesium solution versus the protocol that involves initial ligation in magnesium and repeated ligation in sodium. Therefore, we cannot conclude that magnesium hinders EDC ligation in the DNA crystals.

With validated EDC reaction solution conditions in hand, the roles of sticky base overhang and terminal phosphorylation position were assessed. Crystals containing terminal phosphates only on the crossover strands (S1(5′P or 3′P)-S2-S3) and 1 or 2 nt overhangs were compared (Figure 4A). Again, the optimized EDC conditions were used with one dose

https://doi.org/10.1021/acsnanoscienceau.4c00013
ACS Nanosci. Au 2024, 4, 338−348

Table 3. Distribution of DNA Block Sizes as a Ffunction of Crystal Sticky Base Overhang Length and 3′ vs. 5′ Terminal Phosphates[a]

DNA Crystal Strand 1 Ligation Products (Figure 4A)								
parent DNA	1SB 5′P	1SB 3′P	2SB 5′P	2SB 3′P	1SB 5′P	1SB 3′P	2SB 5′P	2SB 3′P
EDC buffer component	Mg(II)	Mg(II)	Mg(II)	Mg(II)	Na(I)	Na(I)	Na(I)	Na(I)
DNA block size	[%]	[%]	[%]	[%]	[%]	[%]	[%]	[%]
1	51.2	8.4	12.4	8.9	58.6	3.9	6.0	3.5
2	35.0	12.3	41.9	8.1	17.4	8.5	13.9	1.2
3	10.0	10.2	17.6	7.1	11.3	5.8	15.2	8.6
4	3.2	8.7	10.2	7.1	5.0	5.8	13.6	8.0
5	0.7	9.0	6.3	7.2	2.7	8.1	13.0	9.7
6		7.9	4.3	7.2	2.0	8.9	11.9	10.5
7		9.1	3.0	5.3	1.4	8.7	10.5	10.1
8 and above		34.3	4.3	49.3	1.7	50.2	16.0	48.4
Parent DNA	1SB 5′P	1SB 3′P	2SB 5′P	2SB 3′P	1SB 5′P	1SB 3′P	2SB 5′P	2SB 3′P
EDC buffer component	Mg(II)	Mg(II)	Mg(II)	Mg(II)	Na(I)	Na(I)	Na(I)	Na(I)
P_{SSB}[b]	0.598 ± 0.012	0.154 ± 0.004	0.325 ± 0.009	0.140 ± 0.004	0.511 ± 0.014	0.136 ± 0.004	0.205 ± 0.006	0.138 ± 0.004
$P_{LIG} = 1-P_{SSB}$	0.402 ± 0.012	0.846 ± 0.004	0.675 ± 0.009	0.860 ± 0.004	0.489 ± 0.014	0.864 ± 0.004	0.795 ± 0.06	0.862 ± 0.004

[a]Data shown corresponds with the gel lanes in Figure 4A. The cross-linking protocol was four doses of 30 mg/mL EDC for 12 h, and crystal samples were compared after four doses. The EDC buffer component indicates whether the crystal was cross-linked in the presence of magnesium or transferred to a sodium buffer (replacing magnesium). The values in this table are weighted to correct for the linearly increased dye intensity for longer DNA strands. Unweighted values are found in Table S6. The full table including estimated mole fractions for higher-order products is found in Table S7. P_{SSB} and P_{LIG} were calculated for each cross-linked crystal sample. Double strand ligation is not possible here because only Strand 1 was phosphorylated. [b]Calculated from experimental mole fractions per eq 1 (Table 1). PLIG is derived from PSSB as shown.

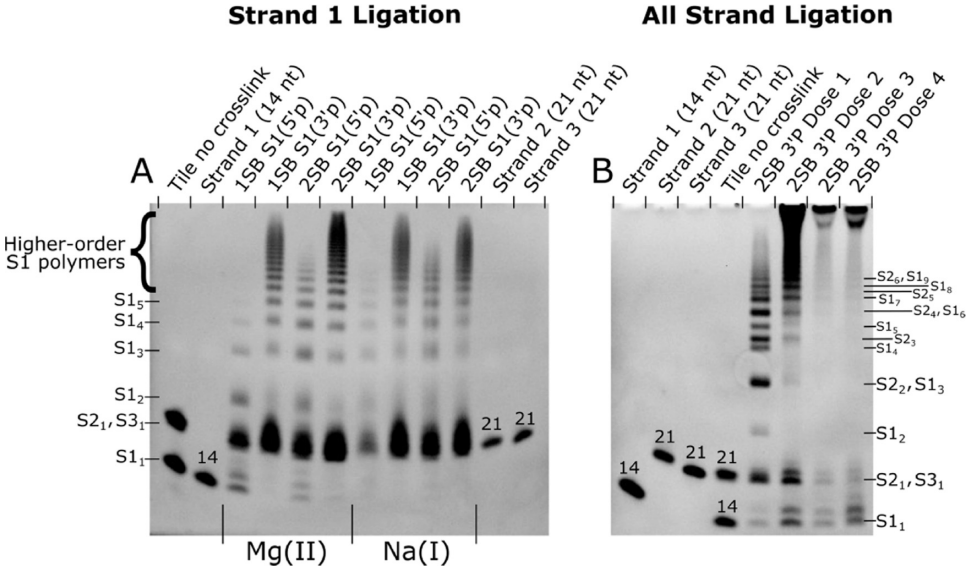

Figure 4. TBE-urea gels of EDC ligation for DNA crystals. Crystals with modifications only on strand 1 are shown (A) with varied sticky base overhangs (1SB and 2SB) and varied terminal phosphates (5′phos or 3′phos) after four doses of EDC. Furthermore, the same crystal classes are compared side-by-side in buffers with Mg(II) or with later rounds of ligation occurring after a buffer exchange into Na(I). Up to four EDC doses were applied to (B) crystals with 2 sticky bases and 3′ phosphates on all strands, revealing an apparent high ligation yield. After three EDC doses, lower-size products disappear except for bands attributed to monomer strands. Assigned band sizes are given in bases. Gel densitometry analysis and band attributions are provided in Figures S7 and S8 and Table 3.

corresponding to 30 mg/mL EDC for 12 h. Crystals were subjected to four doses of EDC, with the first dose in magnesium and subsequent doses in sodium. In Figure 4A, we compare the ligation products after four EDC doses. The Strand 1 ligation product distribution was readily interpretable; due to the lack of Strand 2 and 3 ligation, these strands remained constant at 21 bases, where they did not interfere with densitometry on the remaining ligation product bands.

Like cocrystals, DNA crystal junctions with 3′ terminal phosphates ligated more readily than 5′ terminal phosphates for both sticky base variants (1 nt and 2 nt). In the case of the sticky overhang length, the two sticky base overhangs promoted EDC ligation in the DNA crystals. The increased Strand 1 ligation yields were more prominent between 1nt and 2nt overhangs with 5′ phosphates, where the 1nt 5′phos had ∼49% ligation versus the 2nt 5′phos with ∼80% ligation (Table 3). For further comparison of all four doses of ligation, see Supplemental Figures S4−S5. As discussed in the Supporting Information for our previous report,[26] if ligation is random, then the remaining 1-mer mole fraction after

https://doi.org/10.1021/acsnanoscienceau.4c00013
ACS Nanosci. Au 2024, 4, 338−348

ligation provides another estimate (P_{SSB}') for the total strand break probability. Here, the correlation was reasonably strong (R^2 = 0.8663) between P_{SSB}' and P_{SSB} calculated from the mole fractions via eq 1 (Figure S6). The random ligation model is consistent with the idea that catalysis is slow relative to the intracrystal transport of EDC, so ligation is equally likely to occur throughout the body of the crystal.

Following the comparison of crossover strand (S1) phosphorylation, we sought to achieve a fully ligated crystal with each junction phosphorylated. Crystals containing terminal phosphates on each strand (S1, S2, and S3) were grown, and we assessed gel densitometry results after four EDC doses. In Figure 4B, crystals with 2 sticky base overhangs and 3′ terminal phosphates had efficient ligation in the crystal. A significant quantity of the DNA loaded into these gels appeared to remain in the loading wells. For crystals ligated with 3 or 4 doses, there was additionally a visible band for a distinct long product. Future work may accurately size this long product band (i.e., with a gel that is optimized for longer DNA strands) and identify the constituent strands (e.g., using nanopore long-read sequencing). We hypothesize that the apparent strong ligation yield at higher doses may reflect the entangling of ligated DNA threads, which prevent full denaturation and separation of the crystal into constituent ssDNA strands. The diminishing relative intensity of the $S3_1$ band with repeated ligation doses (relative to) may reflect circularized S3 becoming entangled with longer strands. Entangling complicates attempts to quantify ligation performance. Additionally, as ligation approaches completion, remaining smaller ligation product bands may increasingly reflect finite crystal size effects rather than incomplete ligation chemistry yield. Even in a hypothetical fully ligated crystal, some strands would be short due to intersections with the crystal surfaces. We attribute the notable remaining population of small species as originating from these finite crystal effects or perhaps from incomplete phosphorylation. While we did not attempt to further quantify the ligation yield for crystals subjected to 3 or 4 doses, we were able to estimate the ligation product mole fractions for one or two EDC doses (Table S8). Future work to accurately assess the yield for the in-crystal ligation yield of circular S3 will require solution synthesis of control circular S3 to establish how the circular strand runs on these gels. We also performed the same experiment with 2 sticky base overhangs and 5′ terminal phosphates. As with the Strand 1 ligations, after four EDC doses, the 3′ phosphates resulted in more ligation than the 5′ phosphates (Figure S9).

Further studies are needed to determine the effects of EDC ligation on X-ray diffraction quality for pure DNA crystals. As previously noted by Ohayon et al., tensegrity triangle crystals have marginal X-ray diffraction resolution.[28] In limited testing of the non-cross-linked crystals, we have not obtained diffraction suitable for structure determination. For future investigation of EDC chemical ligation of DNA crystals, it may be advantageous to select an alternative DNA crystal with more favorable initial diffraction.

Post-Ligation Stability in Harsh Conditions

For biomedical applications, engineered biomolecular crystals should be robust in solution conditions other than their growth solutions. After EDC ligation, the cocrystals and DNA crystals were subjected to both an ion-free environment (deionized water) and to blood serum (bovine calf). Cross-linked DNA crystals with 2 sticky base overhangs and 3′ phosphates on each strand with two doses of EDC ligation (sister crystals of the ligation in Figure 4B Lane 6) showed amazing stability in these harsh conditions (in contrast to the immediate destruction of nonligated crystals) (Figure 5). The stability

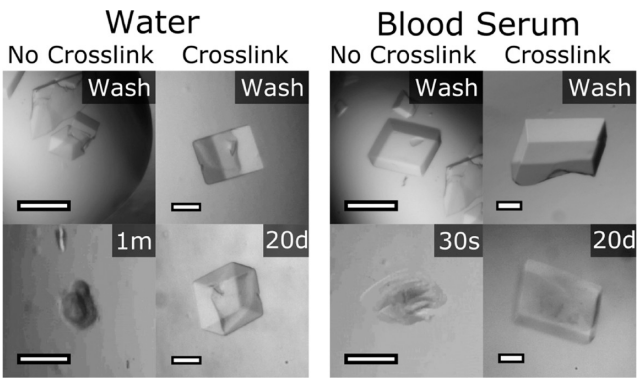

Figure 5. DNA crystals in water and blood serum. Comparison of native and cross-linked crystal stability in harsh conditions. The DNA crystals had 2 sticky base overhangs and 3′ terminal phosphates on each strand (2SB S1(3′P)-S2(3′P)-S3(3′P)). Crystals were cross-linked with 2 doses of 30 mg/mL EDC for 12 h. After quenching the EDC reaction in the tris base, crystals were transferred to the ligation wash solution (without EDC). All scale bars are 100 μm.

in these cross-linked DNA crystals can only be attributed to the addition of ligation (compared to the cocrystals which may also benefit from protein−protein cross-links).

DNA crystals with a terminal phosphate on only strand 1 (2SB S1(3′P)-S2-S3) were also subjected to water and blood serum (Figure S10). When quenching the EDC reaction in 50 mM tris base pH 8.3, the cross-linked DNA crystals (2SB S1(3′P)-S2-S3) visibly cracked. After adding these crystals to water, their macrostructure was expanded and remained as such for 20 days. In blood serum, the cross-linked crystal (2SB S1(3′P)-S2-S3) maintained the parallelepiped macrostructure for 20 days. Tunable degradation may be feasible by tuning the ligation yield, which would enable certain applications (*e.g.*, extended release of therapeutic cargo molecules).

Cocrystals with varied sticky base overhangs and terminal phosphorylation status were subjected to four harsh conditions: ion-free environment (water), blood serum, stomach acid mimic (pH 2.0), and lysosomal fluid mimic (pH 4.5). Non-cross-linked cocrystals degraded rapidly in all four conditions (Figure S11). After the cocrystals were cross-linked with two doses of EDC (30 mg/mL EDC for 12 h), quenched in 50 mM tris base pH 8.0, and washed in a growth solution mimic, the crystals were transferred to the harsh conditions. In Figure 6, we highlight the incredible stability of cross-linked cocrystals with 2 sticky base overhangs and 3′ terminal phosphates. In all four harsh conditions, the crystals maintain their macrostructure after 21 days (albeit with an arguably expanded structure in pH 2.0) (Figures S12−S15). Directly assessing crystal size and shape is challenging due to the crystal habit, which presents a different cross-section shape depending on the viewing angle. In a more detailed analysis (Figures S12−S15), the only crystal that appeared to (arguably) change size was the crystal incubated in pH 2.0, where the unfolding of the protein might be responsible for the size change.

It is important to note that control cocrystals without terminal phosphates were also stabilized by the two doses of EDC ligation. Therefore, we cannot attribute the full stability

https://doi.org/10.1021/acsnanoscienceau.4c00013
ACS Nanosci. Au 2024, 4, 338−348

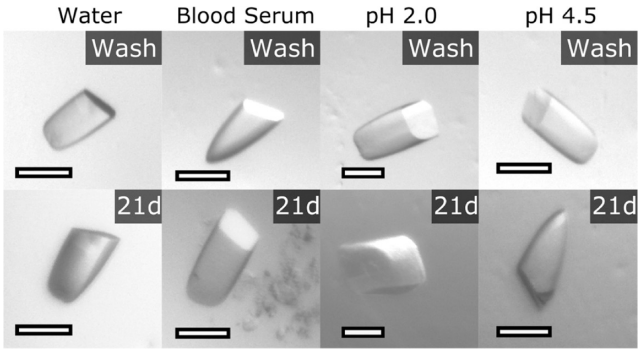

Figure 6. Cross-linked cocrystals in four different harsh conditions. The cocrystals shown have 2 sticky base overhangs and 3′phosphates. Crystals were cross-linked with 2 doses of 30 mg/mL EDC for 12 h. After quenching the EDC reaction in the tris base, crystals were transferred to a ligation wash solution (without EDC). All scale bars are 100 μm.

of the cocrystals to DNA ligation. While some cocrystal stability can be attributed to the protein components, it is not obvious from the crystal structure which intermolecular protein−protein cross-links might be responsible. Regardless, the stability provided by EDC cross-linking in cocrystals may make them useful for biomedical applications.

CONCLUSIONS

In this study, chemical EDC ligation was shown to be effective in two crystal classes that contain DNA blocks stacking end-to-end. The roles of sticky base overhangs and terminal phosphate placement were assessed. In DNA crystals, two-base sticky overhang junctions with 3′terminal phosphates outperformed the alternatives (1 sticky base or 5′ phosphates). With 3′ terminal phosphates at each DNA junction in the DNA crystal, the apparent ligation yield was very high after 3 EDC doses (though bands attributed to monomer strands were still visible, potentially due to finite crystal effects). (Figure 4). In cocrystals, ligation yield trends as a function of sticky overhang length were not readily apparent in gel electrophoresis analysis after one EDC dose. However, after 2 EDC doses, a marked increase in ligation yield was observed for crystals with 2 sticky base overhangs and 3′ terminal phosphates. As in our first study of EDC ligation in cocrystals,[26] 3′ terminal phosphates exceeded the ligation yields of 5′ terminal phosphates.

Advantages of EDC ligation include facile transport into small solvent pores, maintained crystal nanoscale assembly and X-ray diffraction quality, and reaction tunability for the crystal target and crystal application. Additionally, the short half-life of EDC and post-ligation washing of crystals eliminate unreacted carbodiimide as well as the reaction product.[36] Lastly, we note that prior cytocompatibility testing of EDC cross-linked protein crystals revealed negligible toxicity.[37] Li et al. previously ligated *porous* DNA crystals with T4 DNA ligase.[20] While the PDB lacks a crystal structure for the 4-turn DNA crystal ligated by T4 DNA ligase, it surely has a maximum guest diameter that significantly exceeds the maximum guest diameter for the 3-turn DNA crystal (~5.7 nm from the MAP_CHANNELS[35] analysis of PDB entry 3ubi). Here, we show EDC chemical ligation in DNA crystals, a method feasible for crystals with smaller pore sizes. Specifically, we can estimate the maximum solvent channel diameter for the interpenetrating CC1 crystals as ~2 nm using MAP_CHANNELS.[35] We also report successful ligation of each symmetry distinct junction within tensegrity triangle crystals. For engineering purposes, EDC ligation opens the flexibility of terminal phosphorylation status (varying 5′ or 3′ phosphates), and the nick site can hypothetically be in a less accessible site (compared to the case for T4 DNA ligase).

In addition to optimizing the crystal building units for ligation, we found that a gentle buffer exchange was necessary for both crystal types to achieve chemical ligation. Li et al. ligated porous DNA crystals with enzymatic ligation, but they specifically needed to avoid salt concentrations higher than 100 mM Mg(II), as it would interfere with T4 DNA ligase.[20] Although Mg(II) also decreased EDC ligation yields for crystals with 5′ phosphates, we were able to remove Mg(II) for successive cross-linking rounds in pursuit of higher ligation yields.

For biomedical applications, cocrystals were shown to be robust in deionized water, blood serum, and at low pH (pH 2.0 or pH 4.5). Further studies may assess the cytocompatibility of cross-linked DNA crystals and cocrystals *in vivo* for drug delivery. In theory, ligation yields should be tunable for the application needed, including controlled crystal degradation. For some applications, it would be advantageous to reduce the EDC dose to shorten the crystal longevity.

ASSOCIATED CONTENT

Supporting Information

The Supporting Information is available free of charge at https://pubs.acs.org/doi/10.1021/acsnanoscienceau.4c00013.

Results for densitometry, gel electrophoresis results, probability comparison, stability tests, and electron density. Methods for crystal growth, detailed X-ray diffraction data, and unweighted ligation percentage calculations (PDF)

AUTHOR INFORMATION

Corresponding Author

Christopher D. Snow − *Department of Chemistry, Colorado State University, Fort Collins, Colorado 80523, United States; Department of Cell and Molecular Biology, Department of Biomedical Engineering, and Department of Chemical and Biological Engineering, Colorado State University, Fort Collins, Colorado 80523, United States;* orcid.org/0000-0002-7690-3519; Email: christopher.snow@colostate.edu

Authors

Abigail R. Orun − *Department of Chemistry, Colorado State University, Fort Collins, Colorado 80523, United States*

Caroline K. Slaughter − *Department of Cell and Molecular Biology, Colorado State University, Fort Collins, Colorado 80523, United States;* orcid.org/0000-0002-1530-0546

Ethan T. Shields − *Department of Biomedical Engineering, Colorado State University, Fort Collins, Colorado 80523, United States*

Ananya Vajapayajula − *Department of Chemical and Biological Engineering, Colorado State University, Fort Collins, Colorado 80523, United States;* Present Address: Department of Chemical and Biomolecular Engineering, Georgia Institute of Technology, Atlanta, Georgia, 30332, United States. Email: avajapayajula3@gatech.edu; orcid.org/0000-0003-0343-0594

https://doi.org/10.1021/acsnanoscienceau.4c00013
ACS Nanosci. Au 2024, 4, 338−348

Sara Jones − *Department of Chemical and Biological Engineering, Colorado State University, Fort Collins, Colorado 80523, United States*

Rojina Shrestha − *Department of Cell and Molecular Biology, Colorado State University, Fort Collins, Colorado 80523, United States*

Complete contact information is available at: https://pubs.acs.org/10.1021/acsnanoscienceau.4c00013

Author Contributions

The manuscript was written through contributions of all authors. All authors have given approval to the final version of the manuscript. CRediT: **Abigail R. Orun** conceptualization, data curation, formal analysis, methodology, supervision, validation, visualization, writing-original draft, writing-review & editing; **Caroline K. Slaughter** data curation, validation, visualization, writing-original draft, writing-review & editing; **Ethan T. Shields** data curation, formal analysis, validation, writing-original draft, writing-review & editing; **Ananya Vajapayajula** data curation, formal analysis, writing-review & editing; **Sara Jones** data curation, formal analysis, validation, writing-review & editing; **Rojina Shrestha** data curation, formal analysis, writing-original draft; **Christopher D. Snow** conceptualization, funding acquisition, investigation, project administration, supervision, validation, visualization, writing-original draft, writing-review & editing.

Funding

This material is based upon work supported by the National Science Foundation under Grant No. NSF DMR 2003748, NSF DMR 1506219, and NSF DMR 2310574. Author C.K.S. received financial support from a T32 training grant from the National Institutes of Health, GM132057. The team also gratefully acknowledges support for undergraduate researchers from the Nelson Family Faculty Excellence Award.

Notes

The authors declare no competing financial interest.

ACKNOWLEDGMENTS

The authors thank Hataichanok (Mam) Sherman, Director of the Histone Source at Colorado State University for the expression and purification of the RepE54 initiator; Beamline 4.2.2 of the Advanced Light Source, a DOE Office of Science User Facility under Contract No. DE-AC02-05CH11231, is supported in part by the ALS-ENABLE program funded by the National Institutes of Health, National Institute of General Medical Sciences, grant P30 GM124169-01; Jay Nix at the ALS Beamline 4.2.2 for extensive support on XRD data collection; and Shing Ho for correcting a previous mistake in gel interpretation and subsequent ligation yields.

DEDICATION

In memory of Rojina Shrestha who passed away during the preparation of this manuscript on May 29, 2022.

ABBREVIATIONS

EDC, 1-ethyl-3-(3-dimethylaminopropyl)carbodiimide; CC1, Cocrystal 1; S1, Strand 1; S2, Strand 2; S3, Strand 3; PDB, Protein Data Bank

REFERENCES

(1) Rupp, B. *Biomolecular Crystallography*; Garland Science: New York, 2009. DOI: 10.1201/9780429258756.

(2) Li, Z.; Zheng, M.; Liu, L.; Seeman, N. C.; Mao, C. 5′-Phosphorylation Strengthens Sticky-End Cohesions. *J. Am. Chem. Soc.* **2021**, *143* (37), 14987−14991.

(3) Falkner, J. C.; Al-Somali, A. M.; Jamison, J. A.; Zhang, J.; Adrianse, S. L.; Simpson, R. L.; Calabretta, M. K.; Radding, W.; Phillips, G. N.; Colvin, V. L. Generation of Size-Controlled, Submicrometer Protein Crystals. *Chem. Mater.* **2005**, *17* (10), 2679−2686.

(4) Saoji, M.; Zhang, D.; Paukstelis, P. J. Probing the Role of Sequence in the Assembly of Three-Dimensional DNA Crystals. *Biopolymers* **2015**, *103* (11), 618−626.

(5) Kong, H.; Sun, B.; Yu, F.; Wang, Q.; Xia, K.; Jiang, D. Exploring the Potential of Three-Dimensional DNA Crystals in Nanotechnology: Design, Optimization, and Applications. *Adv. Sci.* **2023**, *10* (24), No. 2302021.

(6) Maita, N. Crystal Structure Determination of Ubiquitin by Fusion to a Protein That Forms a Highly Porous Crystal Lattice. *J. Am. Chem. Soc.* **2018**, *140* (42), 13546−13549.

(7) Huber, T. R.; McPherson, E. C.; Keating, C. E.; Snow, C. D. Installing Guest Molecules at Specific Sites within Scaffold Protein Crystals. *Bioconjugate Chem.* **2018**, *29* (1), 17−22.

(8) Ward, A. R.; Snow, C. D. Porous Crystals as Scaffolds for Structural Biology. *Curr. Opin. Struct. Biol.* **2020**, *60*, 85−92.

(9) Ernst, P.; Plückthun, A.; Mittl, P. R. E. Structural Analysis of Biological Targets by Host:Guest Crystal Lattice Engineering. *Sci. Rep.* **2019**, *9* (1), No. 15199.

(10) Kowalski, A. E.; Johnson, L. B.; Dierl, H. K.; Park, S.; Huber, T. R.; Snow, C. D. Porous Protein Crystals as Scaffolds for Enzyme Immobilization. *Biomater. Sci.* **2019**, *7* (5), 1898−1904.

(11) Geng, C.; Paukstelis, P. J. DNA Crystals as Vehicles for Biocatalysis. *J. Am. Chem. Soc.* **2014**, *136* (22), 7817−7820.

(12) Stuart, J. D.; Hartman, D. A.; Gray, L. I.; Jones, A. A.; Wickenkamp, N. R.; Hirt, C.; Safira, A.; Regas, A. R.; Kondash, T. M.; Yates, M. L.; Driga, S.; Snow, C. D.; Kading, R. C. Mosquito Tagging Using DNA-Barcoded Nanoporous Protein Microcrystals. *PNAS Nexus* **2022**, *1* (4), No. pgac190.

(13) Zheng, J.; Birktoft, J. J.; Chen, Y.; Wang, T.; Sha, R.; Constantinou, P. E.; Ginell, S. L.; Mao, C.; Seeman, N. C. From Molecular to Macroscopic via the Rational Design of a Self-Assembled 3D DNA Crystal. *Nature* **2009**, *461* (7260), 74−77.

(14) Woloszyn, K.; Vecchioni, S.; Ohayon, Y. P.; Lu, B.; Ma, Y.; Huang, Q.; Zhu, E.; Chernovolenko, D.; Markus, T.; Jonoska, N.; Mao, C.; Seeman, N. C.; Sha, R. Augmented DNA Nanoarchitectures: A Structural Library of 3D Self-Assembling Tensegrity Triangle Variants. *Adv. Mater.* **2022**, *34* (49), No. 2206876.

(15) Seeman, N. C. Nucleic Acid Junctions and Lattices. *J. Theor. Biol.* **1982**, *99* (2), 237−247.

(16) Paukstelis, P. J.; Seeman, N. C. 3D DNA Crystals and Nanotechnology. *Crystals* **2016**, *6* (8), 97.

(17) Zhang, C.; Zhao, J.; Lu, B.; Seeman, N. C.; Sha, R.; Noinaj, N.; Mao, C. Engineering DNA Crystals toward Studying DNA-Guest Molecule Interactions. *J. Am. Chem. Soc.* **2023**, *145*, 4853−4859.

(18) Orun, A. R.; Shields, E. T.; Dmytriw, S.; Vajapayajula, A.; Slaughter, C. K.; Snow, C. D. Modular Protein-DNA Cocrystals as Precise, Programmable Assembly Scaffolds. *ACS Nano* **2023**, *17* (14), 13110−13120.

(19) Liu, D.; Wang, M.; Deng, Z.; Walulu, R.; Mao, C. Tensegrity: Construction of Rigid DNA Triangles with Flexible Four-Arm DNA Junctions. *J. Am. Chem. Soc.* **2004**, *126* (8), 2324−2325.

(20) Li, Z.; Liu, L.; Zheng, M.; Zhao, J.; Seeman, N. C.; Mao, C. Making Engineered 3D DNA Crystals Robust. *J. Am. Chem. Soc.* **2019**, *141* (40), 15850−15855.

(21) Hermanson, G. T. Bioconjugate Techniques: Third ed.; Academic Press, Boston, 2013. DOI: 10.1016/C2009-0-64240-9.

(22) Zhang, D.; Paukstelis, P. J. Enhancing DNA Crystal Durability through Chemical Crosslinking. *ChemBioChem* **2016**, *17* (12), 1163−1170.
(23) Abdallah, H. O.; Ohayon, Y. P.; Chandrasekaran, A. R.; Sha, R.; Fox, K. R.; Brown, T.; Rusling, D. A.; Mao, C.; Seeman, N. C. Stabilisation of Self-Assembled DNA Crystals by Triplex-Directed Photo-Cross-Linking. *Chem. Commun.* **2016**, *52*, 8014−8017.
(24) Gerling, T.; Kube, M.; Kick, B.; Dietz, H. Sequence-Programmable Covalent Bonding of Designed DNA Assemblies. *Sci. Adv.* **2018**, *4* (8), 1157.
(25) Fraccia, T. P.; Smith, G. P.; Zanchetta, G.; Paraboschi, E.; Yi, Y.; Walba, D. M.; Dieci, G.; Clark, N. A.; Bellini, T. Abiotic Ligation of DNA Oligomers Templated by Their Liquid Crystal Ordering. *Nat. Commun.* **2015**, *6* (1), No. 6424.
(26) Ward, A. R.; Dmytriw, S.; Vajapayajula, A.; Snow, C. D. Stabilizing DNA−Protein Co-Crystals via Intra-Crystal Chemical Ligation of the DNA. *Crystals* **2022**, *12* (1), 49.
(27) Xiu, D.; Zhao, S.; Li, Z.; Xu, Y.; Wang, Y.; Zhu, Z.; Zhang, M.; Snow, C. D.; Belfiore, L. A.; Tang, J. Conditionally Designed Luminescent DNA Crystals Doped by Ln3+(Eu3+/Tb3+) Complexes or Fluorescent Proteins with Smart Drug Sensing Property. *J. Mater. Chem. B* **2022**, *10* (34), 6443−6452.
(28) Ohayon, Y. P.; Hernandez, C.; Chandrasekaran, A. R.; Wang, X.; Abdallah, H. O.; Jong, M. A.; Mohsen, M. G.; Sha, R.; Birktoft, J. J.; Lukeman, P. S.; Chaikin, P. M.; Ginell, S. L.; Mao, C.; Seeman, N. C. Designing Higher Resolution Self-Assembled 3D DNA Crystals via Strand Terminus Modifications. *ACS Nano* **2019**, *13* (7), 7957−7965.
(29) Ward, A. R.; Snow, C. D. *Scripts for Modeling Chemical Ligation of DNA Junctions within Biomolecular Crystals*; Zenodo: Geneva, Switzerland, 2021. DOI: 10.5281/ZENODO.7667968.
(30) Kabsch, W. XDS. *Acta Crystallogr., Sect. D: Biol. Crystallogr.* **2010**, *66* (Pt 2), 125−132.
(31) Liebschner, D.; Afonine, P. V.; Baker, M. L.; Bunkoczi, G.; Chen, V. B.; Croll, T. I.; Hintze, B.; Hung, L. W.; Jain, S.; McCoy, A. J.; Moriarty, N. W.; Oeffner, R. D.; Poon, B. K.; Prisant, M. G.; Read, R. J.; Richardson, J. S.; Richardson, D. C.; Sammito, M. D.; Sobolev, O. V.; Stockwell, D. H.; Terwilliger, T. C.; Urzhumtsev, A. G.; Videau, L. L.; Williams, C. J.; Adams, P. D. Macromolecular Structure Determination Using X-Rays, Neutrons and Electrons: Recent Developments in Phenix. *Acta Crystallogr., Sect. D: Struct. Biol.* **2019**, *75* (10), 861−877.
(32) Emsley, P.; Lohkamp, B.; Scott, W. G.; Cowtan, K. Features and Development of Coot. *Acta Crystallogr., Sect. D: Biol. Crystallogr.* *66* (4): 486−501. .
(33) Gelbin, A.; Schneider, B.; Clowney, L.; Hsieh, S. H.; Olson, W. K.; Berman, H. M. Geometric Parameters in Nucleic Acids: Sugar and Phosphate Constituents. *J. Am. Chem. Soc.* **1996**, *118* (3), 519−529.
(34) Komori, H.; Matsunaga, F.; Higuchi, Y.; Ishiai, M.; Wada, C.; Miki, K. Crystal Structure of a Prokaryotic Replication Initiator Protein Bound to DNA at 2.6 A Resolution. *EMBO J.* **1999**, *18* (17), 4597.
(35) Juers, D. H.; Ruffin, J. MAP-CHANNELS: A Computation Tool to Aid in the Visualization and Characterization of Solvent Channels in Macromolecular Crystals. *J. Appl. Crystallogr.* **2014**, *47* (6), 2105−2108.
(36) Gilles, M. A.; Antoine, Q. H.; Borders, C. L. Stability of Water-Soluble Carbodiimides in Aqueous Solution. *Anal. Biochem.* **1990**, *184* (2), 244−248.
(37) Hartje, L. F.; Bui, H. T.; Andales, D. A.; James, S. P.; Huber, T. R.; Snow, C. D. Characterizing the Cytocompatibility of Various Cross-Linking Chemistries for the Production of Biostable Large-Pore Protein Crystal Materials. *ACS Biomater. Sci. Eng.* **2018**, *4* (3), 826−831.